

Workflow for computational fluid dynamics modeling of fixed-bed reactors packed with metal foam pellets: Hydrodynamics

Geniu R. George¹  | Marina Bockelmann² | Leonhard Schmalhorst³ |
Didier Beton³ | Alexandra Gerstle³ | Lars Torkuhl³ | Andreas Lindermeir² |
Gregor D. Wehinger¹ 

¹Institute of Chemical and Electrochemical Process Engineering, Clausthal University of Technology, Clausthal-Zellerfeld, Germany

²CUTEC Research Centre, Clausthal University of Technology, Clausthal-Zellerfeld, Germany

³Alantum Europe GmbH, Munich, Germany

Correspondence

Geniu R. George, Institute of Chemical and Electrochemical Process Engineering, Clausthal University of Technology, Leibnizstrasse 17, 38678 Clausthal-Zellerfeld, Germany.
Email: george@icvt.tu-clausthal.de

Funding information

Federal Ministry for Economic Affairs and Energy, Grant/Award Number: ZF 4640501VS8

Abstract

In recent years, the catalyst pellets made of open-cell metallic foams have been identified as a promising alternative in fixed-bed reactors. A reliable modeling tool is necessary to investigate the suitability of different foam properties and the shapes of foam pellets. In this article, a workflow for a detailed computational fluid dynamics (CFD) model is presented, which aims to study the flow characteristics in the slender packed beds made of metal foam pellets. The CFD model accounts for the actual random packing structure and the fluid flow throughout the interstitial regions is fully resolved, whereas flow through the porous foam pellets is represented by the closure equations for the porous media model. The bed structure is generated using rigid body dynamics (RBD) and the influence of the catalyst loading method is also considered. The mean bed voidage and the pressure drop predicted by the simulations show good agreement with the experimental data.

KEYWORDS

CFD, fixed-bed reactor, open-cell metal foam, pellets, pressure drop

1 | INTRODUCTION

An open-cell metal foam is a solid cellular structure with a network of inter-connected pores; characterized by high porosity, high specific surface area, and global thermal conductivity, it is felicitous for a wide range of applications.¹ In recent decades, the suitability of metallic foams as catalyst supports has been investigated by many researchers in terms of pressure drop, heat and mass transfer characteristics, as well as chemical reactions.^{2,3}

Meanwhile, the advancement in manufacturing technology has induced the production of pure metallic foams (e.g., Ni, Fe, and Cu) and the alloy compositions (e.g., NiFeCrAl, NiCrAl, Inconel 625, and FeCrAl)

in an economical way as well as being tailored for specific applications.^{4,5} Moreover, the foam sheets can be shaped as drop-in-pellets type for the application in fixed-bed reactors. Figure 1 depicts a few shapes of metal foam pellet realized by Alantum Europe GmbH, Germany, in using a patented manufacturing process.⁶ This design flexibility allows the customization of metal foam pellets to meet the requirements of many industrial processes, where the conventional ceramic pellets have failed to satisfy the entire process demands. Dixon⁷ has identified that the major requirements in large-volume applications like methane steam reforming are of incompatible nature. To feed methane at higher flow rates upon maintaining lower pressure drop prompts the use of large particles, whereas smaller-sized particles

This is an open access article under the terms of the Creative Commons Attribution License, which permits use, distribution and reproduction in any medium, provided the original work is properly cited.

© 2021 The Authors. *AIChE Journal* published by Wiley Periodicals LLC on behalf of American Institute of Chemical Engineers.

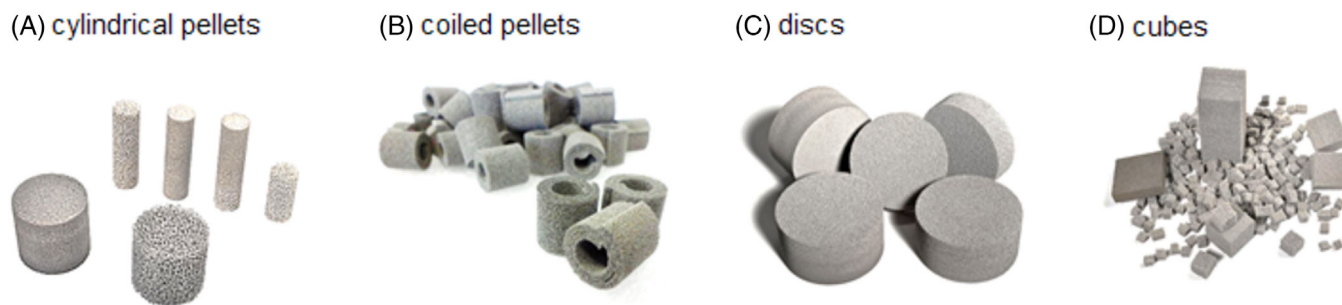


FIGURE 1 Metal foam pellets manufactured by Alantum Europe GmbH, Germany [Color figure can be viewed at wileyonlinelibrary.com]

are beneficial from a reaction perspective, as they provide higher surface area per unit volume of the bed. Furthermore, special attention is needed in the design of fixed-bed reactors to ensure an adequate transport of energy from the reactor wall to the center core of the bed or vice versa. Hence, a low tube-to-particle diameter ratio, $N = D/d_p < 10$, is the preferred choice for the processes which require heating or cooling of the reactor.⁸ Walther et al.⁹ have pointed out that the radial heat transfer performance of a fixed-bed reactor can be enhanced by the use of suitable alloyed metal foam pellets, which also ensure lower pressure drop. Thus, the adoption of metal foam pellets in the fixed-bed reactor is a process intensification approach, since the reactor efficiency is improved, and the operation cost can be reduced.

However, the tortuous inner structure of metallic foam pellets added with considerable internal flow causes a complex flow field compared with conventional nonporous pellets. A thorough understanding of the fluid dynamics of the packing structure composed of metal foam pellets is very important to harness its potential. Indeed, detailed studies pertaining to flow characteristics are scarce. Kolaczowski et al.¹⁰ carried out experiments to measure the pressure drop in a slender-tube fixed-bed reactor made of slab-shaped and cubic metal foam pellets. A significant reduction in pressure drop was observed in comparison to solid counterparts. They also devised a method to determine the proportion of fluid that flows through the pellets, which was quantified up to 38%. This flow distribution is dependent on the arrangement of foam pellets in the reactor column, pellet size or shape, and the foam morphological parameters, mainly cell size, and porosity. Since experimental studies of this kind are time-consuming, reliable modeling tools which provide design and optimization space are necessary to support the development of suitable foam pellet shapes.

The particle-resolved computational fluid dynamics (CFD) approach, which accounts for the actual bed geometry, has been proved as relevant to study the fixed-bed reactors with low N -value.¹¹ At $N < 10$, the influence of the local bed structure is crucial for the local transport phenomena, which can be well predicted with this detailed modeling approach—see the review articles of Dixon and Partopour,¹² and Jurtz et al.¹³ One of the major challenges in the particle-resolved CFD approach is to generate a representative fixed-bed structure. The methods generally used to create packing geometry are tomography scans¹⁴ and by computational methods,^{15–19} in which Discrete Element Method (DEM)^{20,21} and the Rigid Body Dynamics (RBD)^{22,23} method in the framework of the animation software Blender^{24,25} are frequently

used. Recently, Flaischlen and Wehinger²⁶ have carried out a critical evaluation on synthetic bed generation between the DEM method in the commercial software STAR-CCM+ and the RBD approach in Blender. They reported that both methods predict the bed voidage accurately, whereas a more precise prediction of particle orientation in the synthetic beds made of cylinders and hollow cylinders was observed in Blender simulation than in STAR-CCM+, and the latter uses glued-sphere^{27,28} method to model nonspherical particles. In accordance with the previous works, it is confirmed that open-source software Blender integrated with Bullet physics library²⁹ is robust to create synthetic fixed-bed structures for the use in particle-resolved CFD approach.

On the other hand, the high porous nature of the foam materials poses additional challenges in the CFD modeling of the fixed-bed composed of metal foam pellets. It comprises a problem of bi-disperse porous media,³⁰ where the fluid has two flow paths: through and around the porous particles. Pore-scale CFD simulations have been used by many researchers to study the detailed flow characteristics inside the open-cell foam structures, in which the pore-scale geometry is created by either imaging techniques or using idealized foam patterns like kelvin cell, Weaire-Phelan, or random structure.^{31–35} However, this type of detailed CFD simulation is not practically feasible in the packing structures composed of thousands of foam pellets. To address these kinds of problems, multiscale modeling approaches need to be adopted. Recently, Wehinger et al.³⁶ have presented a CFD approach, in which the established particle-resolved CFD model is integrated with pseudo-homogeneous porous medium model to account for the transport phenomena inside the foam pellets. The authors used DEM approach to generate the fixed-bed structure. The pressure drop CFD simulations were compared with the experimental data provided by Kolaczowski et al.¹⁰ and good agreement for medium flow conditions was reported. Along with this, an illustrative heat transfer study highlighted the potential of metal foam pellets in fixed-bed reactors.

In this work, a workflow for an adapted particle-resolved CFD approach is presented to study the flow characteristics in the fixed-bed made of metal foam pellets and validate it against the experimental data of bed voidage and pressure drop. The proposed CFD workflow is similar to Wehinger et al.³⁶; instead of DEM, RBD approach generates the different fixed-bed structures. The inclusion of RBD approach provides more flexibility to model the packing structures with any arbitrary catalyst particle shapes and even allows mimicking the catalyst loading strategies akin to commercial settings, with

low computational efforts. The CFD model is validated against experimental void fraction and pressure drop data for the ceramic Raschig rings and the cylindrical metal foam pellets. It should be noted that the inner structures of the foam pellets are not resolved, whereas flow through the pellets is considered by appropriate closure equations corresponding to the porous media approach. The bed geometry was created using open-source software Blender and the CFD simulations were carried out with Simcenter STAR-CCM+ from Siemens Industry Software Inc. Figure 2 illustrates the proposed CFD workflow. The main objective of this contribution is to develop an adequate CFD model to assist the design of the optimal shape of metal foam pellet.

2 | MATERIALS AND METHODS

2.1 | Pellet characteristics

Two types of catalyst carriers were considered in this study: ceramic Raschig rings and cylindrical metal foam pellets made of NiCrAl alloy (71% Ni, 19% Cr, and 10% Al). Figure 3 illustrates the pellet samples and the definition of important foam morphological parameters. The ceramic Raschig rings were supplied by Vereinigte Füllkörper-Fabriken GmbH & Co. KG, Germany, and the metal foam pellets by Alantum Europe GmbH, Germany.

The characteristic length scale preferred to study the transport phenomena in a fixed-bed reactor is the particle diameter, d_p . In order to compare geometrically different particles, the usual approach is to define equivalent particle diameter in terms of a sphere of equivalent specific surface area, $d_{p,e} = (6V_p/A_p)$. Here, V_p and A_p are the volume and surface area of a particle. Accordingly, the particle Reynolds number is given by Equation (1), where v_s is the superficial velocity and μ is the dynamic viscosity of the fluid medium.

$$Re_p = \frac{\rho v_s d_{p,e}}{\mu} \tag{1}$$

Based on the concept of the hydraulic radius, the Reynolds number complement to the bed structure is dependent on the mean bed voidage, $\bar{\epsilon}_b$, and is related to particle Reynolds number as in Equation (2), which is generally termed as the modified Reynolds number or the bed Reynolds number.^{37,38}

$$Re_p^* = \frac{Re_p}{1 - \bar{\epsilon}_b} \tag{2}$$

Table 1 provides the characteristic dimensions of the pellet samples and the important foam properties. It should be noted that, to define $d_{p,e}$ of the metal foam pellets, only the apparent particle

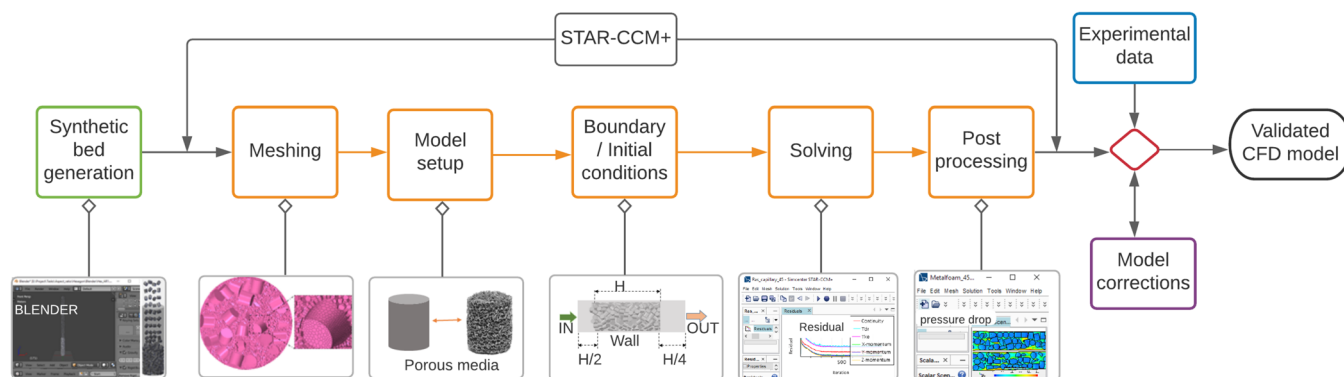


FIGURE 2 Illustration of the proposed CFD workflow [Color figure can be viewed at wileyonlinelibrary.com]

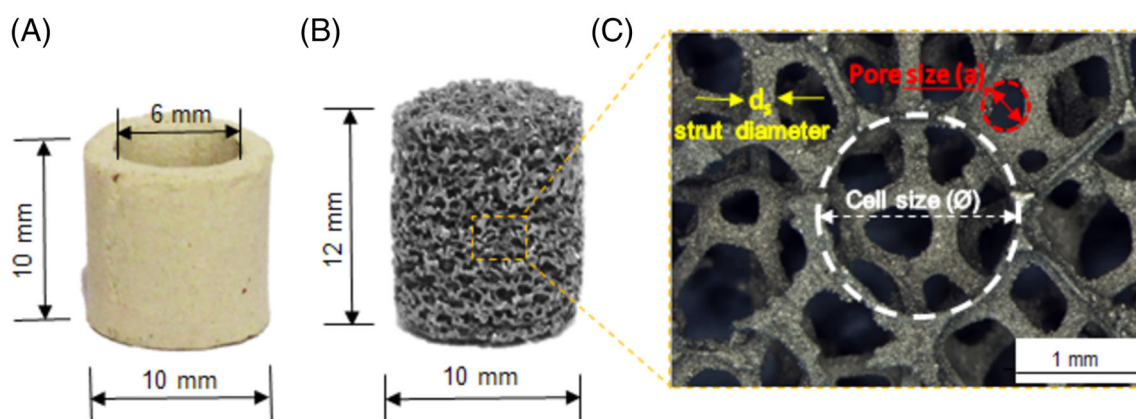


FIGURE 3 (A) Raschig ring, (B) Cylindrical metal foam pellet, and (C) Foam parameters [Color figure can be viewed at wileyonlinelibrary.com]

Pellet types	d_p (mm)	$d_{p,e}$ (mm)	$N^\# = D/d_p$	Cell size (\varnothing) (μm)	Porosity (ϵ)
Raschig ring	10	5	6.78	-	-
Metal foam	10	10.6	6.78	1200 \pm 120	0.87

TABLE 1 Characteristic dimensions and foam properties

Note: # N denotes tube-to-particle diameter ratio; tube diameter, $D = 67.8$ mm.

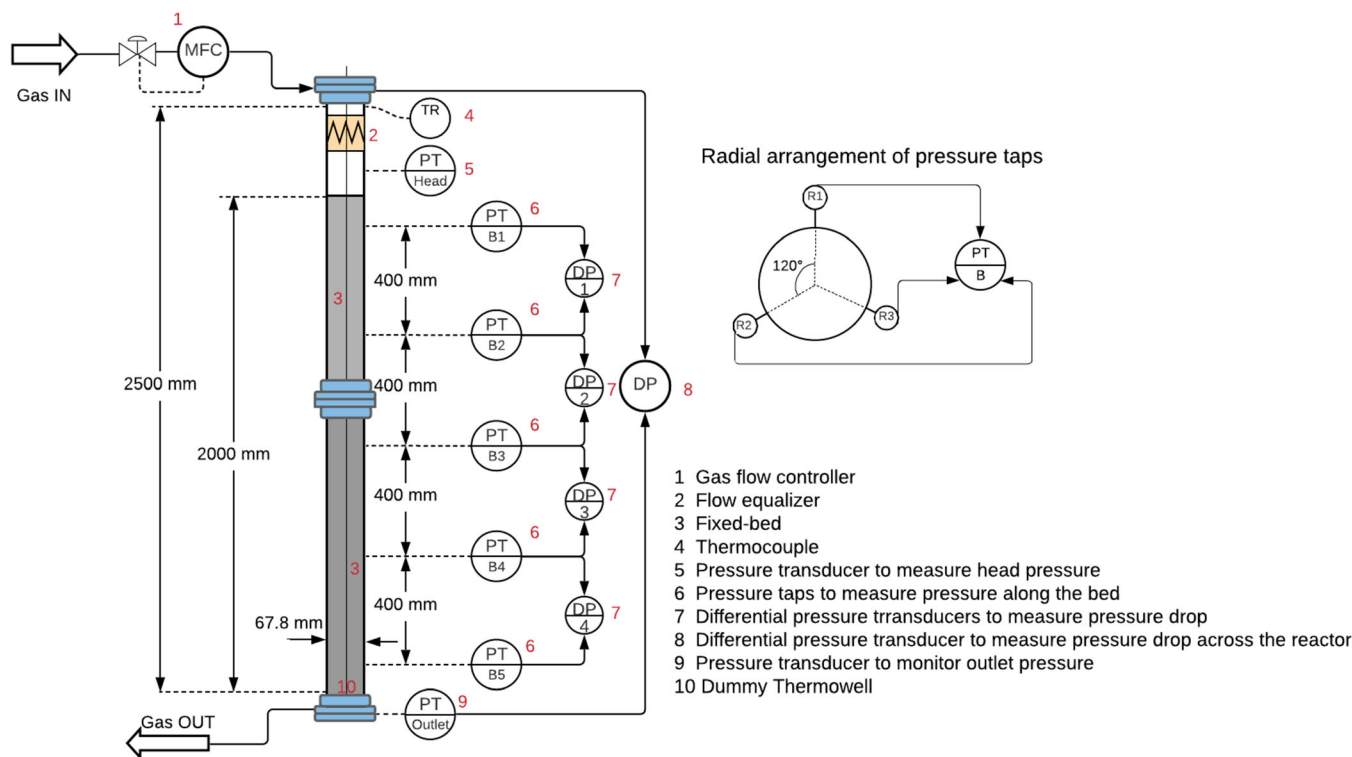


FIGURE 4 Experimental setup with measurement locations [Color figure can be viewed at wileyonlinelibrary.com]

volume and the outer surface area are used, neglecting the particle porosity, ϵ . In addition, the porosity of the foam pellets mentioned in Table 1 does not take into account the micro-voids on the strut surfaces, as they are hardly accessible to fluid flow.³⁹ The pellet samples are not wash-coated, as the present study focuses only on flow behavior under cold flow and nonreactive conditions. Furthermore, wash-coating processes of metal foam pellets might increase the strut thickness, which in turn reduces the overall particle porosity and influences the hydrodynamic quantities as well.¹⁰

2.2 | Experimental setup

A suitable experimental setup for pressure drop measurements was realized and is schematically depicted in Figure 4. The PVC reactor tube has an inner diameter of 67.8 mm and a total height of 2500 mm, comprising two equal segments of 1250 mm. Additionally, a solid steel pipe of diameter 3.5 mm was placed vertically along the center core of the reactor tube to mimic a thermowell, which will be used in the future heat transfer experiments. This PVC reactor is an exact replica of a real metallic reactor proposed for further heat

transfer studies. Onto the top of the reactor tube, a flow equalizer was installed to minimize the flow entry-effects and ensured a uniform or plug-flow-like inlet velocity approaching the top of the bed. The reactor column was filled with pellet samples with the aid of a commercial catalyst loading device (see Supporting Information) up to a maximum height of 2000 mm.

Nitrogen gas was fed at the top of the reactor column and was allowed to flow downwards through the bed. The volumetric flow rate was controlled by a mass flow controller (F-203AV-1M0-RBD-44-V), which has an operating range of 0–45 Nm³/h (Normal conditions: 0°C and 101,325 Pa) and was provided by Bronkhorst Deutschland Nord GmbH, Germany. The flow meter was calibrated on the basis of experiment conditions and the rated accuracy was $\pm (0.8\% \text{ Rd} + 0.2\% \text{ FS})$. The head pressure and the temperature of the feed gas were monitored by a pressure transducer (PT/head—TM-PCE28 0–250 kPa) and a thermocouple (TR—type K), respectively, from Techmark GmbH, Germany, with an accuracy of 0.2% FS. The fluid pressure along the bed was measured by installing pressure taps at five different axial locations, 400 mm apart (PT/B1, PT/B2, PT/B3, PT/B4, and PT/B5). The pressure measured at each axial location was the average of the instantaneous recordings from three pressure taps

that were aligned circumferentially at an angle of 120° apart (see Figure 4). To quantify pressure drop in the bed segments, the corresponding pressure taps at axial locations were connected across the differential pressure transducers (DP/1, DP/2, DP/3, and DP/4—Series 616D 0–20 in w.c). Subsequently, the pressure drop over four-bed segments, each of 400 mm length, was recorded. The differential pressure transducers were provided by Dwyer Instruments, Inc., United States, and the rated accuracy was $\pm 0.25\%$ FS at 25°C. Nitrogen was discharged through the outlet at the very bottom of the reactor column and the outlet pressure was monitored by a pressure transducer (PT/Outlet). Additionally, a differential transducer (DP—TM-AS-dP/0–100 kPa) from Techmark GmbH, Germany, with an accuracy of 0.4% FS was used to monitor the pressure drop across the whole reactor, that is, from inlet to the outlet.

The experiments were conducted at atmospheric pressure and the ambient temperature of about 20°C. The pressure drop data were collected for different mass flow rates in the range of 6.2–56.3 kg/h and the corresponding superficial velocities were between 0.43 and 3.2 m/s, which were calculated based on the ideal gas law connecting temperature and density. The measurements were carried out multiple times at a particular flow rate to ensure repeatability. The behavior of the observed data were also verified in loading and unloading the reactor several times by keeping the same flow parameters. The use of the loading device ensured a high reproducibility of the pressure drop across the bed (see details in the results section).

A unique loading procedure developed by Unidense Technology GmbH, Germany, was adopted to load the pellets, Raschig rings, and foam pellets, in the reactor. This innovative loading device is composed of specially designed springs on a thin flexible loading rope, which ensure controlled loading and the random orientation of pellets in the bed.⁴⁰ This loading device poses several advantages, such as minimum breakage of pellets, least bridging between the pellets, and uniform loading. In industrial applications like methane reforming, the use of a catalyst loading device ensures little variation in pressure drop among the multiple reformer tubes. Additionally, the arrangement of pellets without strong local voids and bridging minimizes the occurrence of temperature hot spots, which in turn favors the catalyst lifetime—see Supporting Information for more details.

2.3 | Synthetic bed generation

In this study, the bed structure was simulated with a rigid body model incorporated in the Bullet physics library,²⁹ which is integrated with the animation software Blender. A detailed description of using Blender for the realization of packing structures has already been addressed.^{24–26} As a starting point, the pellet geometry and the reactor tube were created by the triangular surface meshes. Next, the particles were positioned at the top of the container and allowed to fall freely into the reactor tube. The simulation was proceeded by the physics engine upon resolving the gravity and the interaction forces in discrete time steps. Particle-particle and particle-wall collisions were resolved with the appropriate values of friction and restitution

TABLE 2 RBD parameters used in Blender

Restitution factor	0.7
Friction factor	0.001 to 1
Collision shapes	Convex hull, mesh
Computational time step (s)	0.001
Inner iterations	100
Animation frames	1000–1500

coefficients. Table 2 provides the rigid-body parameters used in this study. The simulations were carried out for a total time of 42 s, where a stable solution of all the balancing forces was attained and consequently, the fixed-bed structure generated—see Supporting Information for more details. Finally, this bed structure was exported as an STL file and imported into the CAE software STAR-CCM+ for the CFD simulations.

The choice of filling strategy and the selection of appropriate rigid body simulation parameters such as the friction coefficient and the restitution factor are debatable. Recently, Jurtz et al.⁴¹ have carried out DEM simulations to generate fixed-beds with a unique catalyst filling strategy. Their study revealed that the mean bed voidage should match between the experimental and the numerical packing, as it is the critical parameter in defining the flow characteristics of a fixed bed. It was also suggested that the static friction coefficient can be used as an adjusting parameter to merge the effects of the loading device, artificial tamping, and the particle surface characteristics. In this way, a filling strategy with less computational effort can be adopted in synthetic bed generation with an adjusted static friction coefficient.

In this study, three filling strategies to generate synthetic beds were compared. A parametric study on friction coefficient was also carried out on each filling strategy. The final selection of the filling strategy and the friction coefficient was carried out by comparing the mean bed voidage of the synthetic bed to the experimental bed and the required computational time. The details are elaborated in Section 3.2.

2.4 | CFD

The flow conditions pertinent to single-phase and turbulent flow were simulated by solving Reynolds-Averaged mass and momentum equations for a 3D domain. The governing equations are presented in the Supporting Information. Realizable $k - \epsilon$ turbulence model,⁴² which computes turbulent viscosity in terms of turbulent kinetic energy and the eddy dissipation rate, was used in this study. The adequacy of the realizable $k - \epsilon$ model in the simulation of fixed-bed reactors has been verified by many authors.¹³

2.4.1 | Modeling flow-through foam pellets

It is computationally challenging to fully resolve the flow field in the inner structures of the foam pellets for an entire bed. Hence, a porous

media model was adopted to mimic flow through the pellets and the corresponding pressure loss. When the flow enters a porous medium, the physical velocity increases due to the reduction in the area available for the flow. The velocity rise is dependent on porosity, ε , which is defined as the ratio of volume available for the fluid flow V_{free} to total volume V , $\varepsilon = (V_{free}/V)$. As a result, the physical velocity, v in a porous medium is related to the superficial velocity as $v_s = \varepsilon v$, which disregards the skeleton of the porous medium and assumes that only the fluid passes through the given cross-sectional area.

The mass and momentum conservation equations in a porous medium based on physical velocity can be formulated as:

$$\frac{\partial(\varepsilon\rho)}{\partial t} + \nabla \cdot (\varepsilon\rho\mathbf{v}) = 0 \quad (3)$$

$$\frac{\partial(\varepsilon\rho)}{\partial t} + \nabla \cdot (\varepsilon\rho\mathbf{v}\mathbf{v}) = -\varepsilon\nabla p + \nabla \cdot (\varepsilon\mathbf{T}) - \varepsilon\mathbf{P}_v\mathbf{v} - \varepsilon\mathbf{P}_i|\mathbf{v}| \quad (4)$$

where \mathbf{P}_v and \mathbf{P}_i are viscous and inertial resistance tensors, respectively. For flow through homogeneous porous media and at very low fluid velocity, the pressure drop is balanced by the viscous shear stress and is linearly proportional to v_s . When the fluid velocity increases, the inertial force starts to contribute and the pressure drop is proportional to v_s^2 . The most widely accepted correlation for predicting the specific pressure drop in an isotropic granular media was suggested by Ergun⁴³ as:

$$\frac{\nabla p}{L} = A \frac{(1-\varepsilon)^2 \mu}{\varepsilon^3 d_{p,e}^2} v_s + B \frac{(1-\varepsilon)\rho}{\varepsilon^3 d_{p,e}} v_s^2 \quad (5)$$

where A is Kozeny-Karman constant and B is Burke-Plummer constant, which should be determined experimentally. For the packed beds, Ergun suggested $A = 150$ and $B = 1.75$. It is clear that the resistance tensors \mathbf{P}_v and \mathbf{P}_i in Equation (4) can easily be equated to Equation (5). On the basis of Ergun-like approach, many authors have proposed pressure drop correlations for the open-cell foam.⁴⁴ The major difficulty in its formulation is to re-define the equivalent particle diameter in terms of the foam morphological parameters such as the strut diameter, d_s and the cell size, \emptyset . A simplistic geometric model, in which a direct analogy between the foam structure and a bed of spherical particles, formulated based on a cubic cell, was proposed by Lacroix et al.³⁹ In this cubic cell model, the foam structure is represented by solid cylindrical filaments connected in 3D as a regular cubic lattice, where the edges symbolize the foam struts. As a result, a relation between strut diameter and particle diameter was developed by equating the specific surface area of the cubic cell to specific surface area of bed of spherical particles as given by Equation (6). The strut diameter is calculated from the cubic cell model based on the porosity, ε and pore diameter a as shown in Equation (7) and Equation (8), where the pore diameter, a , is approximated based on the cell size, \emptyset .

$$d_{p,e} = \frac{6}{4} d_s \quad (6)$$

$$d_s = \frac{a \left[\left(\frac{4}{3\pi} \right) (1-\varepsilon) \right]^{\frac{1}{2}}}{1 - a \left[\left(\frac{4}{3\pi} \right) (1-\varepsilon) \right]^{\frac{1}{2}}} \quad (7)$$

$$a = \frac{\emptyset}{2.3} \quad (8)$$

Transferring Equations (6)–(8) to Equation (5) provide Lacroix correlation, which was applied in this study at each pellet level to account for the corresponding pressure loss of the fluid passing through the open-cell foam pellets. An experimental study was carried out to measure the pressure drop in a single metal foam pellet. The pressure drop predicted by the Lacroix correlation is compared with the experimental data, and an excellent agreement has been found—see Supporting Information.

2.4.2 | Meshing and solution methodology

In order to spatially discretize the computational domain, the meshing process was carried out using the commercial software STAR-CCM+. Polyhedral cells were used in the bulk region and three prism layer cells were considered at the wall of the pellets and the reactor tube. The meshing process in a packed bed is inherently complex due to the presence of the high number of particle-particle and particle-wall contacts, which may lead to local bad cell qualities. To overcome this issue, a meshing procedure by the local cap method was proposed by Eppinger et al.⁴⁵ for the spherical particles and it was extended by Wehinger et al.⁴⁶ for nonspherical particles. The same meshing strategy was followed in this study, which creates a very thin layer of gas-phase cells between very close contacts. The final cell count was ~ 11 million and 16 million for the case of the Raschig ring bed and the metal foam bed, respectively, which has proved sufficient for grid independency in the previous works of similar type.⁴⁷ The meshing details and an overview of the boundary conditions are provided in the Supporting Information.

In line with the experimental studies, Nitrogen gas was considered as the working fluid. At the inlet, a flat velocity profile was assigned with the velocity magnitudes corresponding to the experiment data. No-slip boundary condition was assigned for the reactor wall and the pellet surfaces. The operating pressure and temperature were 101,325 Pa and 298 K, respectively. STAR-CCM+ was used to perform all the CFD simulations, which use the finite-volume method to solve the conservation equations. The closure equations explained in Section 2.4.1 were implemented using field functions in STAR-CCM+. A steady-state simulation was carried out using a segregated flow solver, in which pressure-velocity coupling is based on the SIMPLE algorithm. The convergence was monitored on such solution variables as velocity magnitude and pressure on different positions in the solution domain. In most of the studied cases, convergence criteria were achieved by about 2000 iterations.

3 | RESULTS AND DISCUSSION

3.1 | Experimental pressure drop

The fluid dynamic characteristics of the Raschig ring and metal foam beds are analyzed by taking the experimental data as the basis. Figure 5A,B show the pressure drop measured along with each bed segment for the Raschig ring and the metal foam beds, respectively. It should be noted that the measurements were carried out for repeated trials and a high repeatability of <1% was observed. For the sake of

convenience, the average values are presented, where $\Delta P1$ corresponds to the pressure drop in the bed segment near the inlet and $\Delta P4$ denotes the very bottom bed segment (see Section 2.2 and Figure 4). At a quick glance, the variation in pressure drop along the bed segments is not very significant. However, a slight increase in pressure drop is observed for the downstream bed segments compared with its upstream sections, mainly for higher mass flow rates, > 35 kg/h. The difference is within 4% between the adjacent bed segments and sums up to 6%–9% on comparing the top segment ($\Delta P1$) and the very bottom segment ($\Delta P4$). Interestingly, this trend is almost

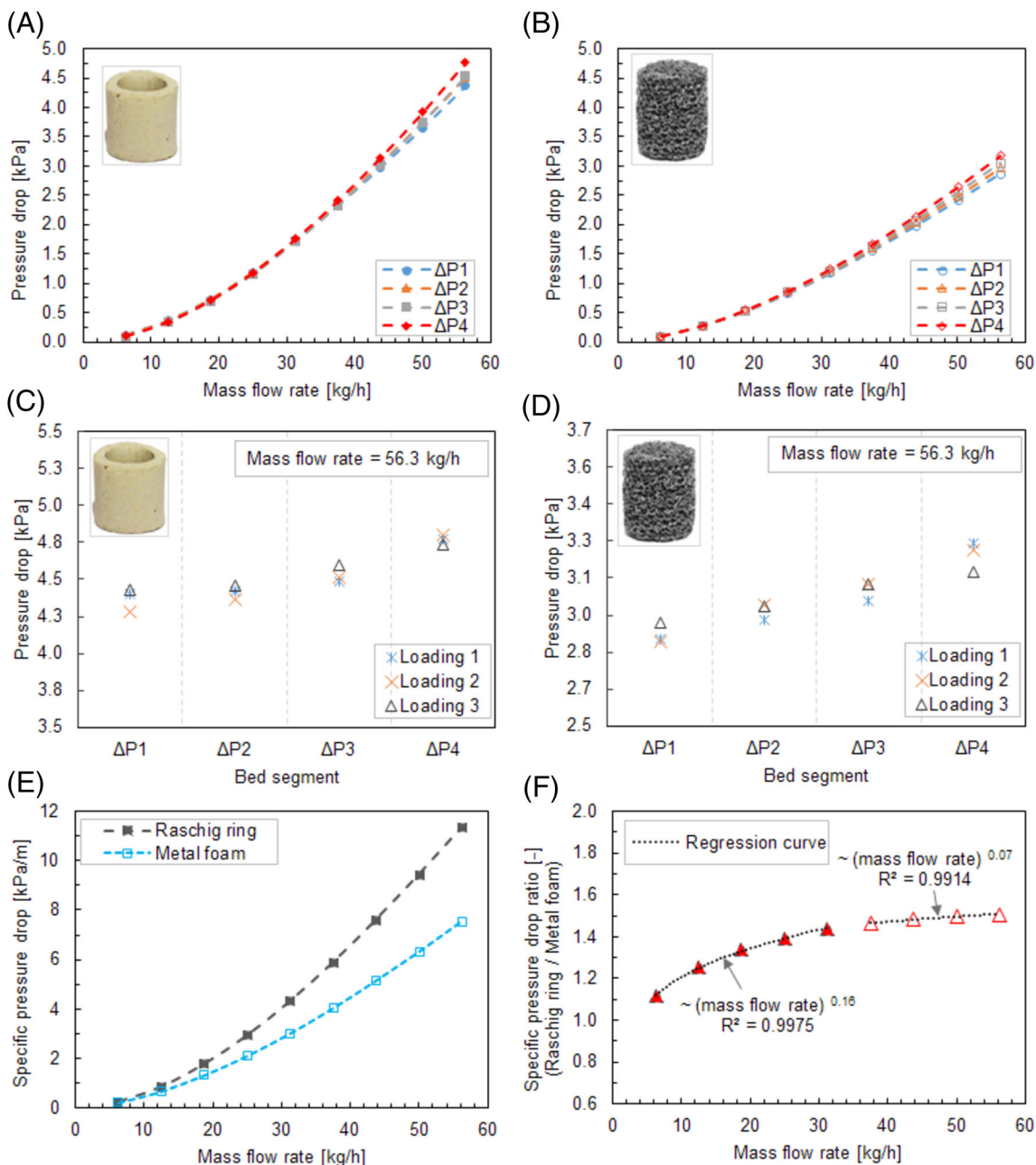


FIGURE 5 Experimental pressure drop across the bed segments: (A) Raschig ring and (B) Metal foam; Experimental pressure drop on repeated loading: (C) Raschig ring and (D) Metal foam; (E) Specific pressure drop along a bed height of 1600 mm; (d) Pressure drop reduction in metal foam pellets as a function of mass flow rate [Color figure can be viewed at wileyonlinelibrary.com]

similar for both the Raschig ring and the metal foam beds. The bottom region of a fixed bed might be denser due to the larger momentum of the particles impacting the bed from a higher altitude. Although this momentum is considerably reduced by the filling device, a difference in bed void fraction over the bed height can be foreseen. Consequently, a pressure drop gradient over the bed segments is also expected. The measurements are also verified upon repeated loading and unloading of the pellets and the results are shown in Figure 5C,D for each bed segment at the maximum mass flow rate of 56.3 kg/h. The variations are not significant ($< 3.5\%$) as the use of a loading device ensures sufficient reproducibility of the packing structure.

For a better comparison, the pressure drop data are normalized by the bed segment length to obtain the specific pressure drop. Figure 5E shows the specific pressure drop in the Raschig ring and metal foam beds, which corresponds to a bed height of 1600 mm (sum of all bed segments). For mass flow rates larger than 10 kg/h, the specific pressure drop of the metal foam bed is considerably lower than that for the bed of Raschig rings. The pressure drop in the Raschig ring bed is about 50% higher compared with the metal foam bed, at the maximum mass flow rate of 56.3 kg/h. In fact, the reduction in pressure drop in the metal foam bed is dependent on the mass flow rate and is depicted in Figure 5F as the ratio of the specific pressure drop in the Raschig ring bed to the metal foam bed. For low to medium flow rates, ≤ 30 kg/h, the variation in the pressure drop is proportional to the mass flow rate with a power factor of 0.16. Afterwards, the factor reduces to 0.07 or exhibits a behavior closer to a linear dependency. The pressure drop in the metal foam bed is dependent on the amount of flow through the pellets. As the

resistance inside the pellets are regulated by flow velocity, the overall flow behavior of a metal foam bed relies on the corresponding flow regime.

3.2 | Validation of synthetic fixed bed structures

The influence of the loading method on the bed structures is investigated by adopting three different filling strategies in Blender simulations and is illustrated in Figure 6: (a) Line-filling, where the pellets are allowed to fall freely from the top of the container in a single line with an imposed random particle orientation; (b) Array-filling being similar to (a), where, instead of a line fashion, the pellets are initialized in an array mode; (c) Pot-Brush-filling, where the pellets are poured into the container from a pot and a brush-like device is used to slowdown the pellets. The brush moves upwards as the bed height increases. This method describes the filling process of the Unidense catalyst loading technology more closely—see Supporting Information.

For all of the loading strategies, a total of 1000 Raschig rings are used and the rigid body parameters are kept the same for all the cases. A dummy thermowell is also considered similar to an experiment, since any type of reactor internals could influence the bed structure. The bed structures generated by using different loading methods and with a constant friction coefficient of 0.7 are also shown in Figure 6. It is observed that the bed generated by the Pot-Brush method is the tallest and is about 13–20 mm higher compared with the beds realized by the Array and the Line methods. This is in line with the observations from Jurtz et al.⁴¹; however, they used a different numerical method (DEM) and a different shape of the filling

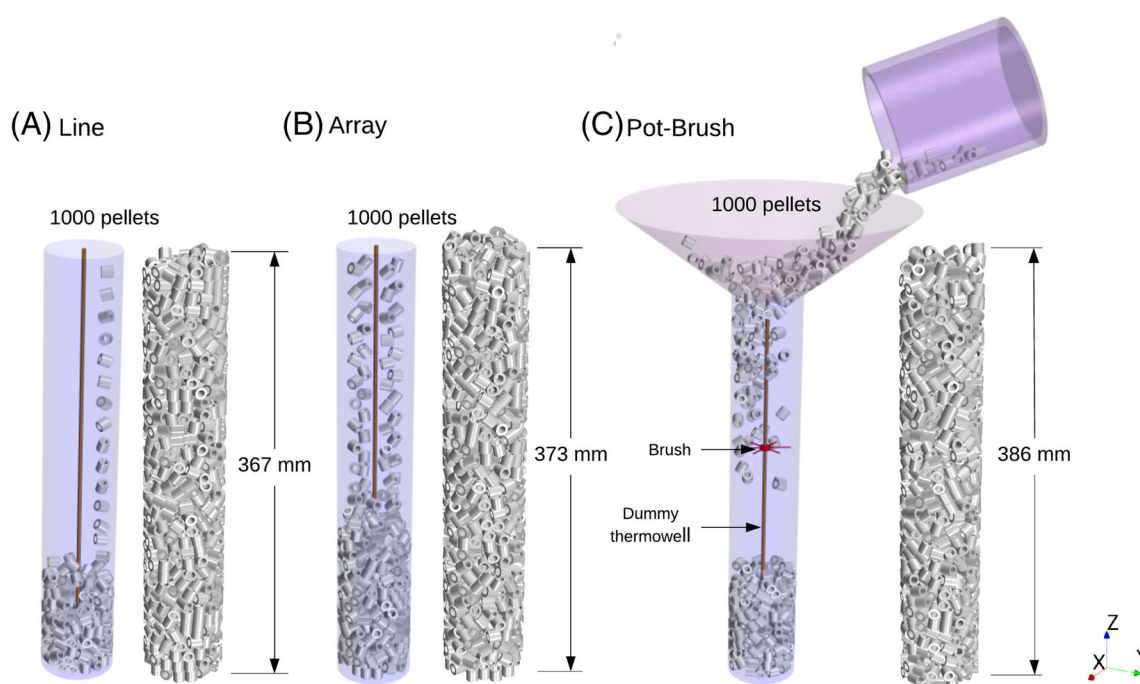


FIGURE 6 Different synthetic filling strategies and corresponding bed structures with a friction coefficient of 0.7: (A) Line, (B) Array, and (C) Pot-Brush [Color figure can be viewed at wileyonlinelibrary.com]

device. In the Pot-Brush method, the brush-like device favors the reduction in the momentum of the falling particles.

In the second step, each of the loading strategies is subjected to a range of friction coefficient and the mean bed voidage of the generated beds is investigated. Figure 7A depicts the comparison of the calculated mean bed voidage for different cases. The general trend is a linear increase in bed voidage while the friction coefficient increases. This is in line with other numerical studies.^{48,49} The friction between the relative contact surfaces is lower at low surface roughness value, which in turn creates denser beds. As far as a comparison of the loading methods is concerned, the Pot-Brush method allows loose beds, whereas the line method results in comparatively denser beds. In Pot-Brush-method, the momentum of the falling particles undergoes reduction upon collision with the brush structure, whereas the momentum gained by the falling particles is higher in the Line-method since there is minimal interaction between the particles on the way into the container. Consequently, the particles may displace more evenly in the bed structure until their momentum dies out. Figure 7A also shows the mean voidage obtained from the experiment and a correlation from the literature.^{50,51} The experimentally derived (based on the weighing method) mean voidage is 0.619 and the corresponding value predicted by the literature correlation is 0.605. The correlation does not account for the capillary inside or the influence of any loading strategy, even though the agreement is satisfactory. From the comparison to the experimental value, it is revealed that the bed generated by the Pot-Brush method with $f = 0.4$ shows good agreement with the experimental value, whereas the Array and Line methods agree to experimental data with $f = 0.7$ and $f = 0.9$, respectively.

The practical applicability of any simulation method has been decided also based on the computational power required for its execution. Here, the computational time taken to simulate each loading strategy is estimated based on one CPU (intel Core i7-8700K) and is depicted in Figure 7B. For the Line and Array methods, the total simulation time is less than an hour, while Pot-Brush requires almost

double the computational power. This is attributed to the extra work of the physics engine to simulate the pouring process of particles from a pot and to simulate the additional collision of particles with the brush structure. Even though, the time consumed for the RBD simulation using Blender is very much lower than the conventional methods like DEM simulations.²⁶

Along with the bed voidage, another important physical parameter of the bed structures made of nonspherical particles is the particle orientation. Moreover, the alignment of particles with respect to the flow direction is more significant when the particles are of hollow type like Raschig rings, multi-hole cylinders, and so forth. Therefore, the impact of the loading methods and the friction coefficient on the orientation of Raschig rings are analyzed with the numerically generated beds. Figure 8A–C show the global particle distribution of orientation for the loading methods Line, Array, and Pot-Brush, respectively. Here, the particle orientation is defined as an angle ($0^\circ \leq \theta \leq 90^\circ$) between the vertical axis of the reactor column and the vertical symmetrical axis of an individual Raschig ring.

It is interesting to note that the predominant particle orientation is 80° – 90° for all the studied cases, which is in line with other experimental observations.¹⁹ The dependency of particle orientation with friction coefficient is almost similar for all the loading methods. The tendency of particles to align either parallel (0° – 10°) or orthogonal (80° – 90°) to the vertical axis is higher for the friction factors < 0.5 . In using the line method, the least particle orientation is in the range (50° – 70°) for all the friction factors. Indeed, for the Array and Pot-Brush methods coupled with friction factors > 0.2 , a minimum number of particles is aligned in the range (0° – 10°). Also, Pot-Brush method allows more particles to align in (40° – 70°) compared with other methods. This reveals that the brush structure helps to align the particles in a more random fashion. Due to the stochastic nature, an exact mathematical formulation for the particle orientation distribution in a random packed bed is cumbersome. It is practically impossible to create an exact replica of particle orientation, while repeating the loading

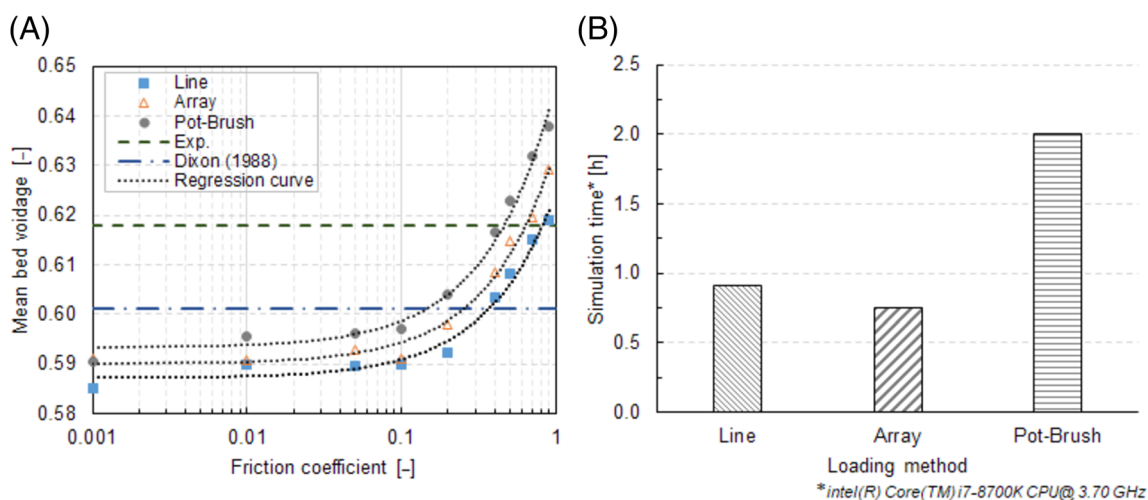


FIGURE 7 (A) Impact of friction coefficient on mean bed voidage; (B) Simulation time versus loading strategy [Color figure can be viewed at wileyonlinelibrary.com]

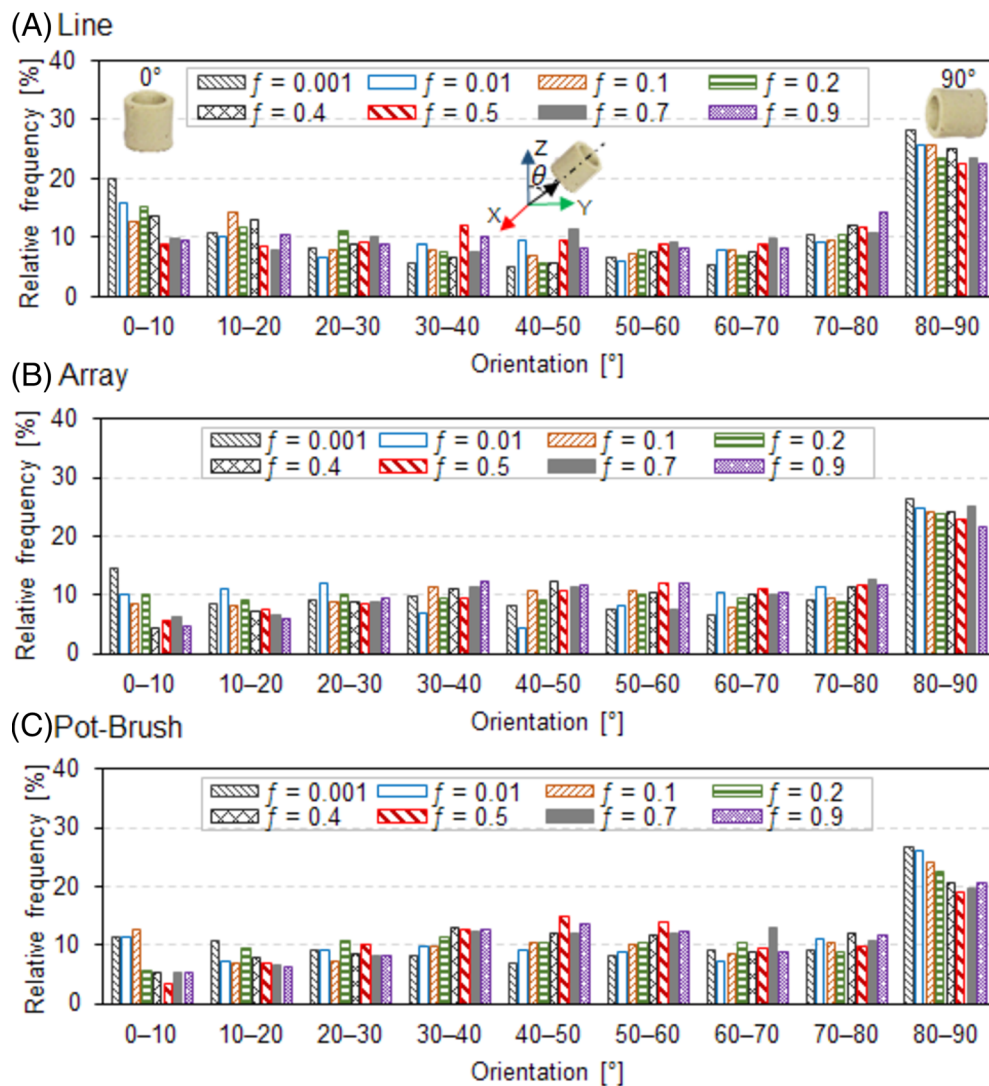


FIGURE 8 Impact of loading strategy and friction factor (f) on particle orientation: (A–C) global orientation distribution for Line, Array, and Pot-Brush, respectively [Color figure can be viewed at wileyonlinelibrary.com]

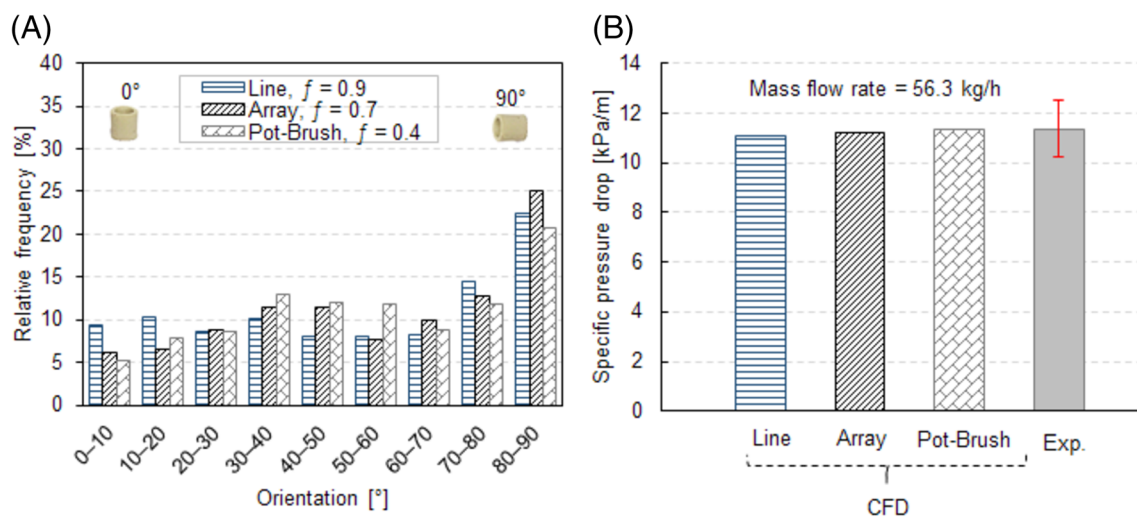


FIGURE 9 (A) Particle orientation in the selected bed structures; (B) Comparison of specific pressure drop in the beds from different loading methods—CFD versus Experiment (error bar of $\pm 10\%$ to cover-up the pressure drop variation along the bed segments and the instrumentation errors) [Color figure can be viewed at wileyonlinelibrary.com]

and unloading of the same packing. Indeed, the overall characteristics can be maintained somewhat similar, that is, the greater tendency to align either perpendicular (90°) or parallel (0°) to the column vertical axis.

As the final step in the validation of the bed structure, a bed from each of the loading strategies is selected, which bears the mean voidage close to the experimental bed, and subjected to pressure drop CFD simulations. Here, it is worthwhile to recall that the mean bed voidage of 0.619 was achieved at friction factors of 0.9, 0.7, and 0.4 for the Line, Array, and Pot-Brush methods, respectively (see Figure 7A). However, the orientation of particles in these beds are not exactly similar as depicted in Figure 9A. The pressure drop simulated by using the numerical bed from each loading strategy is compared with the experimental data for a mass flow rate of 56.5 kg/h and is shown in Figure 9B. An error bar of $\pm 10\%$ is included along with the experimental data to cover up the variation in pressure drop along with the bed segments and other possible instrumentation errors. A very good agreement is observed for all the cases as the deviations are even less than 3%. Hence, it is inferred that the mean bed voidage is the critical parameter in defining the pressure drop characteristics of fixed beds. Furthermore, the effects of catalyst loading device on bed morphology can be included in numerical bed generation by adjusting the RBD parameter: friction coefficient, in a simple loading strategy which is of less computational cost. In this case, Array method is found as efficient from the practical perspective, as it consumes lesser computational time (see Figure 7B) as well as being capable of simulating a bed morphology close to experimental bed.

The Array-method is then extended to generate a representative bed structure for the metal foam pellets. It should be noted that the numerical bed for the metal foam pellets is made of solid cylinders, as flow through the pellets is accounted by the porous media model (see Section 2.4.1). As explained earlier, the friction coefficient is adjusted to achieve a mean bed voidage close to the experimental bed made of metal foam pellets—see Supporting Information.

3.3 | Validation of the CFD model

The validation of the CFD simulation is carried out using the experimental pressure drop data discussed in Section 3.1. Firstly, the ability of particle-resolved CFD approach in predicting the pressure drop of fixed-beds is validated. Figure 10A depicts the comparison of specific pressure drop predicted in the Raschig ring bed to the experimental data. The CFD results show an excellent agreement with the experimental data.

A comparison with empirical correlations proposed by Ergun⁴³ and Nemeć and Levec³⁸ is also carried out. It is evident that Ergun correlation under-predicts pressure drop, whereas Nemeć and Levec over-predicts with a mean relative error of 36% and 21%, respectively. The pressure drop characteristics in a fixed-bed composed of hollow particles and the case of low tube-to-particle diameter ratio were not explicitly considered in arriving the constants in Ergun equation, that is, $A = 150$, $B = 1.75$, see Equation (5). Nevertheless, the equivalent particle term in Ergun equation allows to include the effect of high surface area and the shape effects augmented by the hollow particles to some extent. However, it is not sufficient to incorporate all the flow artifacts occurring in the fixed-beds made of hollow particles. Several experimental studies have shown that the pressure drop in the Raschig ring beds are much higher than anticipated due to the eddies and dead spaces in the inner hole. The correlation of Nemeć and Levec has addressed this issue by the correction in the effective porosity as proposed by Sonntag,⁵² which considers that only 20% of the inner hole volume is subjected to flow. In Figure 10A, the fraction of the inner hole available to fluid flow is designated as “ m ”. Nevertheless, the applicability of a constant m -value for a wide range of flow velocities and different types of hollow cylinders is dubious. The fluid velocity and the size of inner holes could impact the flow through the rings. Importantly, the experimental data used in the realization of Nemeć and Levec correlation are in the flow rate range, $10 \leq Re_p^* \leq 500$. It is also evident from Figure 10A that Nemeć and

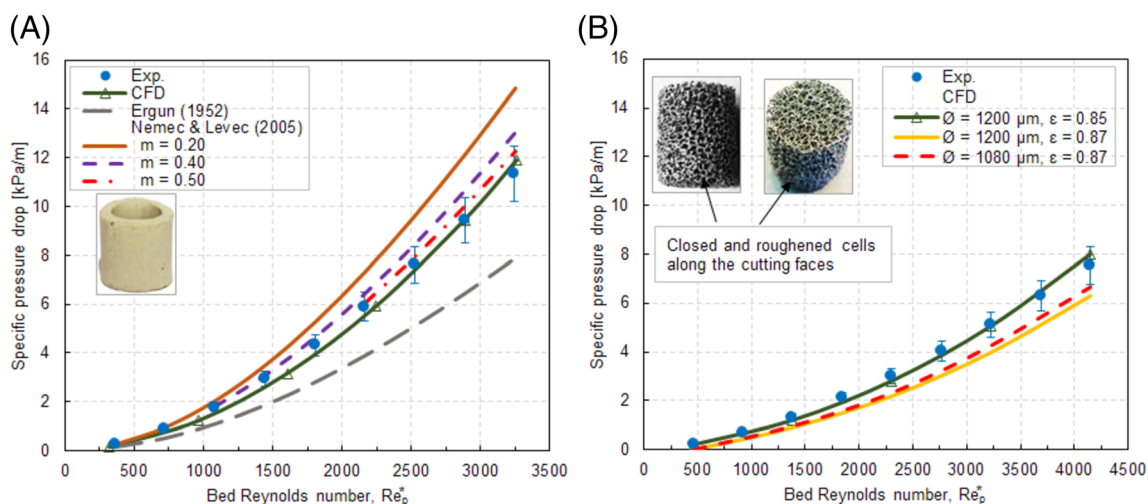


FIGURE 10 Pressure drop comparison: (A) Raschig ring and (B) Metal foam (error bar of $\pm 10\%$ to cover-up the pressure drop variation along the bed segments and the possible instrumentation errors in the experiment) [Color figure can be viewed at wileyonlinelibrary.com]

Levec correlation with $m = 0.20$ predicts pressure drop well for $Re_p^* < 1000$ in comparison to the experimental data; afterwards deviation in prediction increases. A better agreement to the experimental data are observed with the modified m -values of 0.40 in the range, $1000 \leq Re_p^* \leq 2000$ and 0.50 for $2000 < Re_p^* \leq 3250$. The other possible reason for the discrepancies might be the impact of the dummy thermowell. Dixon and Wu⁵³ have investigated the influence of different sizes of thermowells on fluid flow and heat transfer in the fixed-beds. They concluded that the conduction and flow by-passing along the thermowell alter the temperature profile compared with the bed structure without a thermowell. In a recent study of the same authors, an exothermic chemical reaction is considered, and the influence of thermowell in the mass and heat transfer processes under the reaction conditions has also been confirmed.⁵⁴ The presence of the thermowell at the center core of the bed imparts an additional bypass-flow through its circumferential region, where the local bed void fraction is higher. The bypass flow effects are predominant at higher flow rates and, therefore, the deviations are more noticed at higher flow velocity. From this study, it is noteworthy that the particle-resolved CFD is very effective in predicting the flow characteristics of slender fixed-bed reactors with reasonable accuracy and could also be beneficial in understanding the impact of such additional internals as sensors, thermowell, capillaries, and the like.

To predict the pressure drop in metal foam pellets, the validated particle-resolved CFD model for ceramic Raschig ring is adapted with the closure equations explained in Section 2.4.1. The comparison of CFD results to experimental data are shown in Figure 10B. It is observed that the CFD predictions with the foam structural parameters, $\varnothing = 1200 \mu\text{m}$ and $\epsilon = 0.87$ are about 16%–30% lower compared with the experimental data for the range of flow rates investigated. The reliability of the Lacroix correlation (Equations (6)–(8)) in predicting pressure drop of a foam structure greatly depends on the accuracy of the used morphological parameters. However, foams may exhibit considerable variation in their structures, mainly due to the manufacturing routes. The supplier of these foam pellets has accepted an allowance of $\pm 10\%$ in cell size. As shown in Figure 10B, the simulated specific pressure drop with 10% reduction in cell size, that is, $1080 \mu\text{m}$, is closer to experimental data, with a relative error of 12%–25%.

The process of shaping a required pellet geometry from the foam sheet may also affect the physical characteristics of pellets' outer faces. It should be noted that the required height or diameter of a foam pellet has been achieved by stacking thin layers of multiple foam sheets and are adhered to them by heat treatment processes. The thickness of a single layer depends on its cell size and is around 3 mm for the case of $1200 \mu\text{m}$. In the end, the required pellet shapes have been cut out from the thickened sheet.⁵ Upon physical examination of the processed pellets, it is revealed that there are more closed and roughened cells along with the cutting faces as a side-effect of the shaping process (see Figure 10B). This change in foam morphology can cause an additional increase in the pressure drop by reducing the effective porosity. Moreover, the roughened wall surfaces combined with the fine structures of the metal foam pellets might induce additional flow artifacts in the packed bed arrangement that are difficult to reproduce completely in a

CFD framework with the porous-media model. To account for these flow artifacts in the CFD model, a correction factor which modifies the original porosity is applied. As depicted in Figure 10B, CFD results with 2.3% reduction in original porosity, that is, 0.87 to 0.85, showing an excellent agreement with the experimental data. Meanwhile, the suitability of the same correction factor for different foam morphologies and pellet shapes is questionable. This embarks further investigation on the pressure drop characteristics of various pellets shapes and foam morphologies and it will be addressed in a future work.

3.4 | CFD flow field analysis

A detailed study of the flow field is very important to analyze the performance of a reactor. However, experimental insights are very difficult to achieve. The contour maps of velocity magnitude normalized by the superficial velocity of 3.8 m/s are shown in Figure 11A,B, along a vertical section of the Raschig ring and the metal foam beds, respectively. The localized rise in interstitial velocity is clearly visible on both the beds and is proportional to local bed voidage. The regions close to the reactor wall and the dummy thermowell are subjected to significant velocity fluctuations where flow channeling occurs. At $v_s = 3.8 \text{ m/s}$, the local rise in physical velocity can go up by a factor of eight in the Raschig ring, whereas by a factor of about five in the metal foam bed. Since the foam pellets support internal flow, a more homogenous velocity distribution is observed in the metal foam bed, except for the regions close to the wall—see Supporting Information. However, fluid particles experience different resistances while flowing around and through the particles and it is strongly related to the actual foam morphological parameters, mainly cell size, and porosity. The significance of particle orientation is also evident from the contour plots of the Raschig ring bed (see Figure 11A). The inner holes are subjected to considerable fluid flow when it is parallel to the flow direction. Despite, the majority of Raschig rings are aligned perpendicular to the flow direction and are exposed to the eddies and the flow obstructions induced by the upstream particles. Therefore, only a fraction of the inner hole regions could support the fluid flow and, subsequently, the effective bed porosity is reduced.

A qualitative estimation of the amount of flow through the pellets is carried out using CFD simulations. To quantify flow through the pellets, a few cross-sectional planes are selected along the bed, where the average flow velocity in the porous pellet region and the corresponding flow area is calculated. Figure 12A illustrates the streamlines injected from the reactor inlet, and the selected planes for mass flow calculation are shown in Figure 12B. It should be highlighted that the illustrated streamlines could not reflect the real flow tortuosity inside the pellets. Figure 12C depicts the percentage of total fluid flows through the pellets at different bed Reynolds numbers. For the studied cases, the estimated mean mass flow rate is in the range of 21%–33% of the total flow and is dependent on the Reynolds number, see also Equation (5). Indeed, mass flow through the pellets seems relatively constant at $Re_p^* \geq 2000$. This is in line with the results presented by Kolaczowski et al.,¹⁰ which is based on

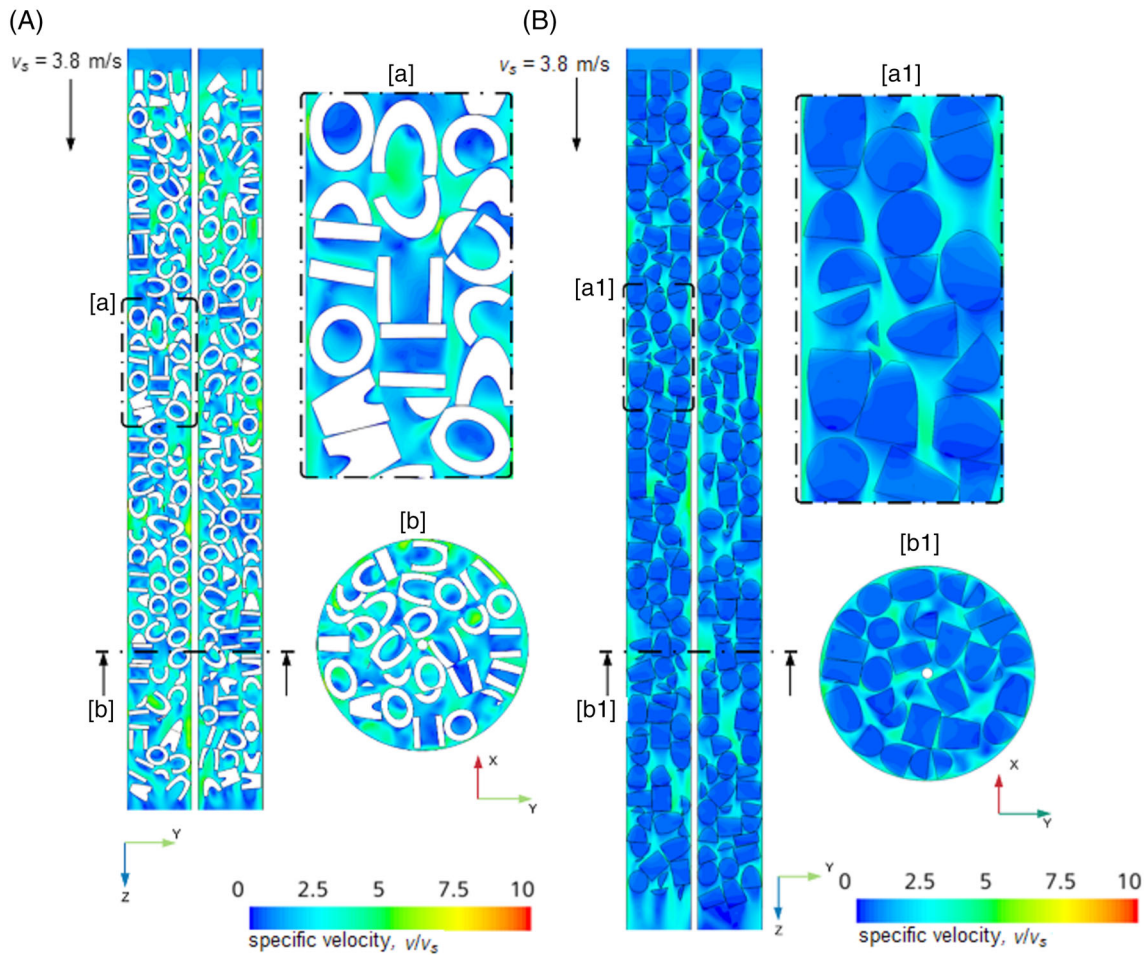
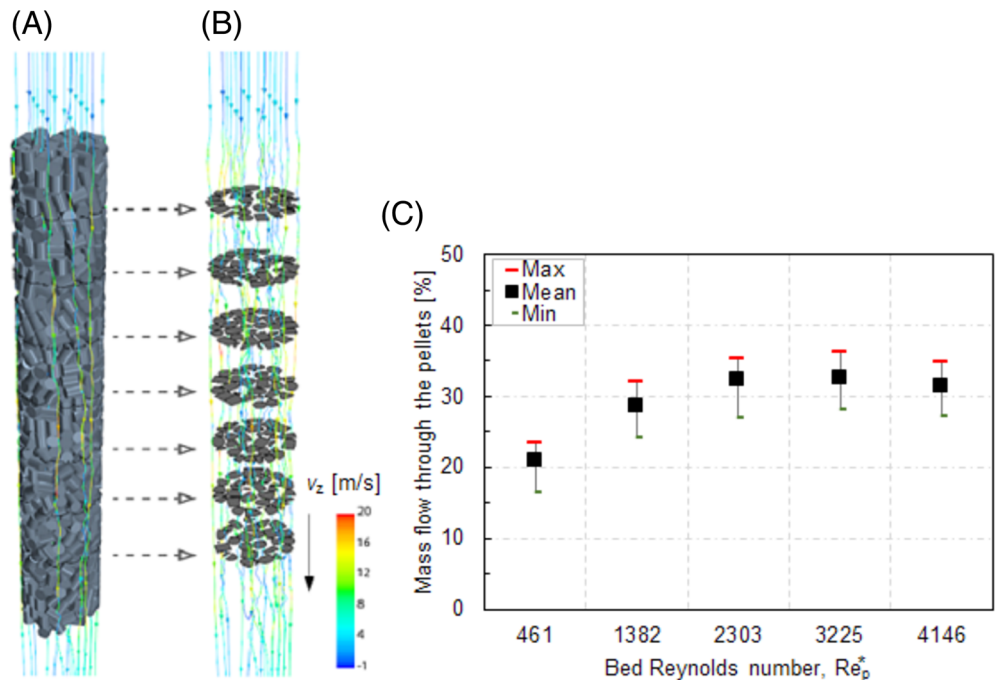


FIGURE 11 Normalized velocity contours (A) Raschig ring (B) Metal foam [Color figure can be viewed at wileyonlinelibrary.com]

FIGURE 12 (A) Representation of streamlines over the bed, (B) Selected planes to calculate the mass flow through the pellets, and (C) Mass flow through pellets as a function of Reynolds number (error bar indicates the fluctuations from different planes) [Color figure can be viewed at wileyonlinelibrary.com]



the experimental studies. It should be kept in mind that, inside the pellets for high velocities, inertia forces dominate the flow resistance via Equation (5). In the interstitial region, pressure drop originates from deflection and detachment of the flow. Hence, the ratio between the flow through and around the pellets depends on the flow regime. However, pore-scale simulations are necessary to limit the uncertainties in modeling the flow through the pellets.

4 | CONCLUSION

An adapted particle-resolved CFD workflow is presented to study the flow characteristics of fixed-bed reactors with randomly packed metal foam pellets. The validation of the CFD model was carried out with the experimental pressure drop data for ceramic Raschig rings and cylindrical metal foam pellets. From the experimental study, it is revealed that pressure drop in the metal foam pellets are lower compared with the Raschig ring. The metal foam pellets are heavily porous, which allows considerable internal flow, subsequently low-pressure drop. By virtue of internal flow and convection around the particles, metal foam pellets could offer an improved fluid–solid interfacial exchange in comparison with conventional ceramic pellets.

We showed that the catalyst loading methods can also be modeled along with synthetic bed generation in using RBD approach integrated in Blender software, with low computational efforts. It should be noted that the mean bed voidage is the critical parameter relevant to the fluid dynamic characteristics of a packing structure. Therefore, the mean bed voidage of the numerical bed should be in good agreement with the real packing structure. It has been achieved by adjusting one of the RBD parameters, that is, friction coefficient, regardless of the catalyst loading method.

In comparison to the experimental data of Raschig rings, the pressure drop predicted by the established particle-resolved CFD approach shows an excellent agreement. It is also evident that detailed CFD simulations could capture even the intrusive effects of measuring devices like the thermowell. The validated particle CFD model is then adapted to mimic the internal flow through the pellets with appropriate closure equations, which are dependent on foam morphological parameters such as cell size and foam porosity. The pressure drop predicted by the adapted CFD model shows good agreement to experimental data in using a modified porosity, which also considers the impact of closed cells along with the cutting faces of the foam pellets in the effective bed voidage.

The flow distribution in the fixed-beds composed of metal foam pellets is highly dependent on the foam morphology. Therefore, it is recommended to verify the applicability of the proposed CFD workflow in different foam morphologies and pellet shapes. This will be addressed in future works. Additionally, the proposed CFD workflow will be extended to study the heat transfer characteristics and chemical reactions.

ACKNOWLEDGMENT

The authors kindly acknowledge the financial support provided by the Federal Ministry for Economic Affairs and Energy (BMWi) under

the funding program—ZIM (Zentrales Innovationsprogramm Mittelstand), Funding No.: ZF 4640501VS8.

AUTHOR CONTRIBUTIONS

Ginu R. George: Conceptualization; data curation; formal analysis; investigation; methodology; validation; visualization; writing-original draft; writing-review & editing. **Marina Bockelmann:** Data curation; formal analysis; investigation; validation; visualization; writing-review & editing. **Leonhard Schmalhorst:** Investigation; project administration; supervision; writing-review & editing. **Didier Beton:** Data curation; funding acquisition; investigation; project administration; supervision; writing-review & editing. **Alexandra Gerstle:** Investigation; project administration; resources. **Lars Torkuhl:** Funding acquisition; project administration; resources; supervision. **Andreas Lindermeir:** Data curation; investigation; project administration; resources; supervision; validation; writing-review & editing. **Gregor D. Wehinger:** Conceptualization; data curation; formal analysis; funding acquisition; investigation; methodology; project administration; resources; supervision; writing-review & editing.

DATA AVAILABILITY STATEMENT

The data that support the findings of this study are available from the corresponding author upon reasonable request.

ORCID

Ginu R. George  <https://orcid.org/0000-0001-6935-629X>

Gregor D. Wehinger  <https://orcid.org/0000-0002-1774-3391>

REFERENCES

1. Banhart J. Manufacture, characterisation and application of cellular metals and metal foams. *Prog Mater Sci.* 2001;46(6):559-632.
2. Giani L, Groppi G, Tronconi E. Mass-transfer characterization of metallic foams as supports for structured catalysts. *Ind Eng Chem Res.* 2005;44(14):4993-5002.
3. Lu TJ, Stone HA, Ashby MF. Heat transfer in open-cell metal foams. *Acta Mater.* 1998;46(10):3619-3635.
4. Kim S, Lee C-W. A review on manufacturing and application of open-cell metal foam. *Procedia Mater Sci.* 2014;4:305-309.
5. Walther G, Klöden B, Büttner T, et al. A new class of high temperature and corrosion resistant nickel-based open-cell foams. *Adv Eng Mater.* 2008;10(9):803-811.
6. Choi B, Kim JK, Bae J, et al., Inventors; Alantum Europe GmbH. Method for producing a pellet, pellet, catalyst charge, and static mixer. United States US 20190388867A1. 2019.
7. Dixon AG. CFD study of effect of inclination angle on transport and reaction in hollow cylinder catalysts. *Chem Eng Res and Des.* 2014;92(7):1279-1295.
8. Dixon AG. Fixed bed catalytic reactor modelling—the radial heat transfer problem. *Can J Chem Eng.* 2012;90(3):507-527.
9. Walther G, Gaitzsch U, Büttner T, Kieback B, Weissgaerber T. *Applications of Metal Foam as Catalyst Carrier.* In: Euro PM2017 Congress & Exhibition. EPMA; 2017. <https://www.epma.com/publications/euro-pm-proceedings/product/ep17-3685867>.
10. Kolaczowski ST, Awdry S, Smith T, Thomas D, Torkuhl L, Kolvenbach R. Potential for metal foams to act as structured catalyst supports in fixed-bed reactors. *Catal Today.* 2016;273:221-233.
11. Partopour B, Dixon AG. 110th anniversary: commentary: CFD as a modeling tool for fixed bed reactors. *Ind Eng Chem Res.* 2019;58(14):5733-5736.

12. Dixon AG, Partopour B. Computational fluid dynamics for fixed bed reactor design. *Annu Rev Chem Biomol Eng.* 2020;11:109-130.
13. Jurtz N, Kraume M, Wehinger GD. Advances in fixed-bed reactor modeling using particle-resolved computational fluid dynamics (CFD). *Rev Chem Eng.* 2019;35(2):139-190.
14. Zhang W, Thompson KE, Reed AH, Beenken L. Relationship between packing structure and porosity in fixed beds of equilateral cylindrical particles. *Chem Eng Sci.* 2006;61(24):8060-8074.
15. Bertei A, Chueh C-C, Pharoah JG, Nicolella C. Modified collective rearrangement sphere-assembly algorithm for random packings of nonspherical particles: towards engineering applications. *Powder Technol.* 2014;253:311-324.
16. Marek M. Numerical generation of a fixed bed structure. *Chem Process Eng.* 2013;34(3):347-359.
17. Marek M. Numerical modeling of random packed beds of various packing densities with a sequential deposition algorithm. *AIP Confer Proceed.* 2019;2078:20015. <https://doi.org/10.1063/1.5092018>.
18. Niegodajew P, Marek M. Analysis of orientation distribution in numerically generated random packings of Raschig rings in a cylindrical container. *Powder Technol.* 2016;297:193-201.
19. Caulkin R, Jia X, Xu C, et al. Simulations of structures in packed columns and validation by X-ray tomography. *Ind Eng Chem Res.* 2009;48(1):202-213.
20. Cundall PA, Strack ODL. A discrete numerical model for granular assemblies. *Géotechnique.* 1979;29(1):47-65.
21. Wehinger GD, Eppinger T, Kraume M. Evaluating catalytic fixed-bed reactors for dry reforming of methane with detailed CFD. *Chem Ing Tech.* 2015;87(6):734-745.
22. Bender J, Erleben K, Trinkle J. Interactive simulation of rigid body dynamics in computer graphics. *Comput Graphics Forum.* 2014;33(1):246-270.
23. Glatt M, Kull D, Ravani B, Aurich JC. Validation of a physics engine for the simulation of material flows in cyber-physical production systems. *Procedia CIRP.* 2019;81:494-499.
24. Boccardo G, Augier F, Haroun Y, Ferré D, Marchisio DL. Validation of a novel open-source work-flow for the simulation of packed-bed reactors. *Chem Eng J.* 2015;279:809-820.
25. Partopour B, Dixon AG. An integrated workflow for resolved-particle packed bed models with complex particle shapes. *Powder Technol.* 2017;322:258-272.
26. Flaischlen S, Wehinger GD. Synthetic packed-bed generation for CFD simulations: Blender vs. STAR-CCM+. *Chem Eng.* 2019;3(2):52.
27. Zhong W, Yu A, Liu X, Tong Z, Zhang H. DEM/CFD-DEM modelling of non-spherical particulate systems: theoretical developments and applications. *Powder Technol.* 2016;302:108-152.
28. Kruggel-Emden H, Rickelt S, Wirtz S, Scherer V. A study on the validity of the multi-sphere discrete element method. *Powder Technol.* 2008;188(2):153-165.
29. Coumans E. *Bullet Physics Library.* 2012. Available at: <http://www.bulletphysics.org>.
30. Yu B, Cheng P. A fractal permeability model for bi-dispersed porous media. *Int J Heat Mass Transf.* 2002;45(14):2983-2993.
31. Wehinger GD, Heitmann H, Kraume M. An artificial structure modeler for 3D CFD simulations of catalytic foams. *Chem Eng J.* 2016;284:543-556.
32. Tucker JC, Spear AD. Correction to: a tool to generate grain-resolved open-cell metal foam models. *Integr Mater Manuf Innovat.* 2019;8(3):440.
33. Bracconi M, Ambrosetti M, Maestri M, Groppi G, Tronconi E. A systematic procedure for the virtual reconstruction of open-cell foams. *Chem Eng J.* 2017;315:608-620.
34. Das S, Deen NG, Kuipers JAM. Direct numerical simulation for flow and heat transfer through random open-cell solid foams: development of an IBM based CFD model. *Catal Today.* 2016;273:140-150.
35. de Carvalho TP, Morvan HP, Hargreaves DM, Oun H, Kennedy A. Pore-scale numerical investigation of pressure drop behaviour across open-cell metal foams. *Transp Porous Media.* 2017;117(2):311-336.
36. Wehinger GD, Kolaczowski ST, Schmalhorst L, Beton D, Torkuhl L. Modeling fixed-bed reactors from metal-foam pellets with detailed CFD. *Chem Eng J.* 2019;373:709-719.
37. Achenbach E. Heat and flow characteristics of packed beds. *Exp Thermal Fluid Sci.* 1995;10(1):17-27.
38. Nemeč D, Levec J. Flow through packed bed reactors: 1. Single-phase flow. *Chem Eng Sci.* 2005;60(24):6947-6957.
39. Lacroix M, Nguyen P, Schweich D, Pham Huu C, Savin-Poncet S, Edouard D. Pressure drop measurements and modeling on SiC foams. *Chem Eng Sci.* 2007;62(12):3259-3267.
40. Ryntveit G, Bayer Kr, NORSK HYDR a.s Method for filling particulate material into tubes. European Patent Office EP 0548999 B1. 30.06.
41. Jurtz N, Wehinger GD, Srivastava U, Henkel T, Kraume M. Validation of pressure drop prediction and bed generation of fixed-beds with complex particle shapes using discrete element method and computational fluid dynamics. *AIChE J.* 2020;66(6):e16967. <https://doi.org/10.1002/aic.16967>.
42. Mohammadi B, Pironneau O. *Analysis of the K-epsilon turbulence model.* France: Editions MASSON; 1993.
43. Ergun S. Fluid flow through packed columns. *Chem Eng Prog.* 1952;48:89-94.
44. Kumar P, Topin F. State-of-the-art of pressure drop in open-cell porous foams: review of experiments and correlations. *J Fluids Eng.* 2017;139(11):5202.
45. Eppinger T, Seidler K, Kraume M. DEM-CFD simulations of fixed bed reactors with small tube to particle diameter ratios. *Chem Eng J.* 2011;166(1):324-331.
46. Wehinger GD, Fütterer C, Kraume M. Contact modifications for CFD simulations of fixed-bed reactors: cylindrical particles. *Ind Eng Chem Res.* 2017;56(1):87-99.
47. Wehinger GD. Particle-resolved CFD simulations of catalytic flow reactors. [PhD Thesis] TU Berlin; 2016.
48. Jurtz N, Waldherr P, Kraume M. Numerical analysis of the impact of particle friction on bed Voidage in fixed-beds. *Chem Ing Tech.* 2019;91(9):1260-1266.
49. Flaischlen S, Kutscherauer M, Wehinger GD. Local structure effects on pressure drop in slender fixed beds of spheres. *Chem Ing Tech.* 2020;93(1-2):273-281.
50. Dixon AG. Correlations for wall and particle shape effects on fixed bed bulk voidage. *Can J Chem Eng.* 1988;66(5):705-708.
51. Foumeny EA, Benyahia F. Predictive characterization of mean voidage in packed beds. *Heat Recovery Syst CHP.* 1991;11(2/3):127.
52. Sonntag G. Einfluß des Lückenvolumens auf den Druckverlust in gasdurchströmten Füllkörpersäulen. *Chem Ing Tech.* 1960;32(5):317.
53. Dixon AG, Wu Y. Flow and heat transfer in narrow fixed beds with axial thermowells. *Numer Heat Transfer, Part A.* 2019;76(11):811-829.
54. Dixon AG, Wu Y. Partial oxidation of o-xylene to phthalic anhydride in a fixed bed reactor with axial thermowells. *Chem Eng Res Des.* 2020;159:125-137.

SUPPORTING INFORMATION

Additional supporting information may be found online in the Supporting Information section at the end of this article.

How to cite this article: George GR, Bockelmann M, Schmalhorst L, et al. Workflow for computational fluid dynamics modeling of fixed-bed reactors packed with metal foam pellets: Hydrodynamics. *AIChE J.* 2021;e17284. <https://doi.org/10.1002/aic.17284>